Interactions in Single Wall Carbon Nanotubes/Pyrene/Porphyrin Nanohybrids

ARTICLE *in* JOURNAL OF THE AMERICAN CHEMICAL SOCIETY · SEPTEMBER 2006

Impact Factor: 12.11 · DOI: 10.1021/ja0624974 · Source: PubMed

12 AUTHORS, INCLUDING:

Francesco Paolucci
University of Bologna
187 PUBLICATIONS **5,633** CITATIONS
SEE PROFILE

Massimo Marcaccio
University of Bologna
131 PUBLICATIONS **4,021** CITATIONS
SEE PROFILE

Manuel Melle-Franco
University of Minho
43 PUBLICATIONS **897** CITATIONS
SEE PROFILE

J|A|C|S
ARTICLES
Published on Web 08/05/2006

Interactions in Single Wall Carbon Nanotubes/Pyrene/Porphyrin Nanohybrids

Christian Ehli,[†] G. M. Aminur Rahman,[†] Norbert Jux,[‡] Domenico Balbinot,[‡] Dirk M. Guldi,*[,†] Francesco Paolucci,[§,⊥] Massimo Marcaccio,[§,⊥] Demis Paolucci,[§] Manuel Melle-Franco,[§,⊥] Francesco Zerbetto,[§,⊥] Stéphane Campidelli,[∥] and Maurizio Prato[∥,⊥]

Contribution from the Institute for Physical and Theoretical Chemistry, Egerlandstrasse 3, 91058 Erlangen, Germany, Institute for Organic Chemistry, Henkestrasse 42, 91054 Erlangen, Germany, Dipartimento di Chimica "G. Ciamician", Università di Bologna, V. F. Selmi 2, I-40126 Bologna, Italy, Consorzio Interuniversitario Nazionale per la Scienza e Tecnologia dei Materiali, Units of Bologna and Trieste, Italy, and Dipartimento di Scienze Farmaceutiche, Università di Trieste, Piazzale Europa 1, I-34127, Trieste, Italy

Received April 19, 2006; E-mail: dirk.guldi@chemie.uni-erlangen.de

Abstract: This work provides an in-depth look at a range of physicochemical aspects of (i) single wall carbon nanotubes (**SWNT**), (ii) pyrene derivatives (**pyrene**$^+$), (iii) porphyrin derivatives (**ZnP**$^{8-}$ and **H$_2$P**$^{8-}$), (iv) poly(sodium 4-styrenesulfonate), and (v) their combinations. Implicit in their supramolecular combinations is the hierarchical integration of **SWNT** (as electron acceptors), together with **ZnP**$^{8-}$ or **H$_2$P**$^{8-}$ (as electron donors), in an aqueous environment mediated through **pyrene**$^+$. This supramolecular approach yields novel electron donor−acceptor nanohybrids (**SWNT/pyrene**$^+$**/ZnP**$^{8-}$ or **SWNT/pyrene**$^+$**/H$_2$P**$^{8-}$). In particular, we report on electrochemical and photophysical investigations that as a whole suggest sizeable and appreciable interactions between the individual components. The key step to form **SWNT/pyrene**$^+$**/ZnP**$^{8-}$ or **SWNT/pyrene**$^+$**/H$_2$P**$^{8-}$ hybrids is $\pi-\pi$ interactions between **SWNT** and **pyrene**$^+$, for which we have developed for the first time a sensitive marker. The marker is the monomeric pyrene fluorescence, which although quenched is (i) only present in **SWNT/pyrene**$^+$ and (ii) completely lacking in just **pyrene**$^+$. Electrostatic interactions help to immobilize **ZnP**$^{8-}$ or **H$_2$P**$^{8-}$ onto **SWNT/pyrene**$^+$ to yield the final electron donor−acceptor nanohybrids. A series of photochemical experiments confirm that long-lived radical ion pairs are formed as a product of a rapid excited-state deactivation of **ZnP**$^{8-}$ or **H$_2$P**$^{8-}$. This formation is fully rationalized on the basis of the properties of the individual moieties. Additional modeling shows that the data are likely to be relevant to the SWNTs present in the sample, which possess wider diameters.

Introduction

Carbon nanotubes (CNTs) are essentially a sheet of carbon atoms arranged in hexagons that curl into a tube. They come in two basic varieties: single wall carbon nanotubes (SWNTs), which are single coils of carbon hexagons, and multiwall carbon nanotubes (MWNTs), wherein single tubes are encased in wider tubes, which themselves are inside other tubes. Most of today's research concentrates on SWNTs, because they have been better characterized and possess characteristic fingerprints in several analytical and spectroscopic techniques.

Considerable efforts have been devoted to integrate the outstanding physicochemical properties of CNTs, either SWNTs or MWNTs, into practical and useful devices. To name only a few of the remarkable features of these nanostructures, CNTs exhibit quasi-ballistic conductance, high tensile strength, and field-effect transistor properties.[1] They also have a high potential for photovoltaic applications, which, however, has received more limited attention.[2] This is due to the difficulties of processing

[†] Institute for Physical and Theoretical Chemistry.
[‡] Institute for Organic Chemistry.
[§] Università di Bologna.
[⊥] Consorzio Interuniversitario Nazionale per la Scienza e Tecnologia dei Materiali.
[∥] Università di Trieste.

(1) (a) Special issue on Carbon Nanotubes. *Acc. Chem. Res.* **2002**, *35*, 997. (b) Reich, S.; Thomsen, C.; Maultzsch, J. *Carbon Nanotubes: Basic concepts and Physical Properties*; Wiley-VCH: Weinheim, Germany, 2004. (c) Dresselhaus, M. S.; Dresselhaus, G.; Avouris, P. *Carbon Nanotubes: Synthesis, Structure, Properties and Applications*; Springer: Berlin, 2001. (d) Harris, P. J. F. *Carbon Nanotubes and Related Structures: New Materials for the Twenty-First Century*; Cambridge University Press: Cambridge, U.K., 2001. (e) Yu, M. F.; Files, B. S.; Arepalli, S.; Ruoff, R. S. *Phys. Rev. Lett.* **2000**, *84*, 5552. (f) Ijima, S.; Brabec, C.; Maiti, A.; Bernholc, J. *J. Chem. Phys.* **1996**, *104*, 2089. (g) Treacy, M. M. J.; Ebbesen, T. W.; Gibson, T. M. *Nature* **1996**, *381*, 678. (h) Falvo, M. R.; Clary, G. J.; Taylor, R. M.; Chi, V.; Brooks, F. P.; Washburn, S.; Superfine, R. *Nature* **1997**, *389*, 582. (i) Huxtable, S. T.; Cahill, D. G.; Shenogin, S.; Xue, L.; Ozisik, R.; Barone, P.; Usrey, M.; Strano, M. S.; Siddons, G.; Shim; M.; Keblinski, P. *Nat. Mater.* **2003**, *2*, 731. (j) Zhang, H. L.; Li, J. F.; Yao, K. F.; Chen, L. D. *J. Appl. Phys.* **2005**, *97*, 114310. (k) Kim, P.; Shi, L.; Majumdar, A.; McEuen, P. L. *Phys. Rev. Lett.* **2001**, *87*, 215502. (l) Hone, J.; Batlogg, B.; Benes, Z.; Johnson, A. T.; Fischer, J. E. *Science* **2000**, *289*, 1730. (m) Misewich, J. A.; Avouris, P.; Martel, R.; Tsang, J. C.; Heinz, S.; Tersoff, J. *Science* **2003**, *300*, 783. (n) De Jonge, N.; Allioux, M.; Doytcheva, M.; Kaiser, M.; Teo, K. B. K.; Lacerda, R. G.; Milne, W. I. *Appl. Phys. Lett.* **2004**, *85*, 1607. (o) Jo, S. H.; Wang, D. Z.; Huang, J. Y.; Li, W. Z.; Kempa, K.; Ren, Z. F. *Appl. Phys. Lett.* **2004**, *85*, 810. (p) Yoon, S. M.; Chae, J.; Suh, J. S. *Appl. Phys. Lett.* **2004**, *84*, 825. (q) Buldum, A.; Lu, J. P. *Phys. Rev. Lett.* **2003**, *91*, 236801/1. (r) Hirsch, A. *Angew. Chem., Int. Ed.* **2002**, *35*, 1853.

10.1021/ja0624974 CCC: $33.50

these highly intractable carbon nanostructures and of obtaining batches with a homogeneous, narrow distribution of tubes diameters.

Recently, scattered examples have been reported of electron donors (i.e., ferrocene, 4-(*N*,*N*-dimethylamino)phenyl, etc.) covalently linked to CNTs.[3] However, their weak absorption cross section, especially in the visible region of the solar spectrum, calls for photosensitization with visible light absorbers. This is a crucial step that precludes the charge separation process in CNTs. In this context, porphyrins and metalloporphyrins, synthetic analogues of natural chlorophylls, represent molecules of choice. Several ways have been explored to integrate porphyrins, metalloporphyrins, or both with CNTs. In general, they fall into two categories: (i) covalently linked CNT nanoconjugates[4] and (ii) noncovalently associated CNT nanohybrids.[5] The latter method appears particularly promising since the covalent approach causes a partial loss of the electronic properties of the functionalized CNT. In previous, recent work, we have shown that the noncovalent combination of SWNTs or MWNTs with porphyrins leads to nanohybrids, which, upon photoexcitation, undergo fast electron transfer followed by the generation of microsecond-lived charge-separated species.[6] Further integration of these systems onto a photoactive electrode, has allowed us to prepare photoelectrochemical cells with relatively high efficiencies.[7] To improve the performance of these systems, a comprehensive understanding of the individual processes that are involved is necessary. The intent is to improve the photoconversion efficiency of our multifunctional hybrid cells.

In this paper, a detailed summary of ground- and excited-state interactions between the individual building blocks, see Scheme 1, is presented in the case of single wall carbon nanotubes (**SWNT**), 1-(trimethylammonium acetyl) pyrene (**pyrene**$^{+}$), and 5,15-bis-[2′,6′-bis-{2″,2″-bis-(carboxy)-ethyl}-methyl-4′-*tert*-butyl-phenyl]-10,20-bis-(4′-*tert*-butylphenyl) porphyrin octasodium (**H_2P^{8-}**) salt and the related zinc complex (**ZnP^{8-}**). A variety of steady-state and time-resolved techniques are employed to test these vastly different absorbing/fluorescing building blocks and their mutual interactions.

Scheme 1. Molecular Building Blocks (i.e., **SWNT**, **SWNT/Pyrene**$^{+}$, and **SWNT/Pyrene**$^{+}$**/ZnP**$^{8-}$) Used in This Work

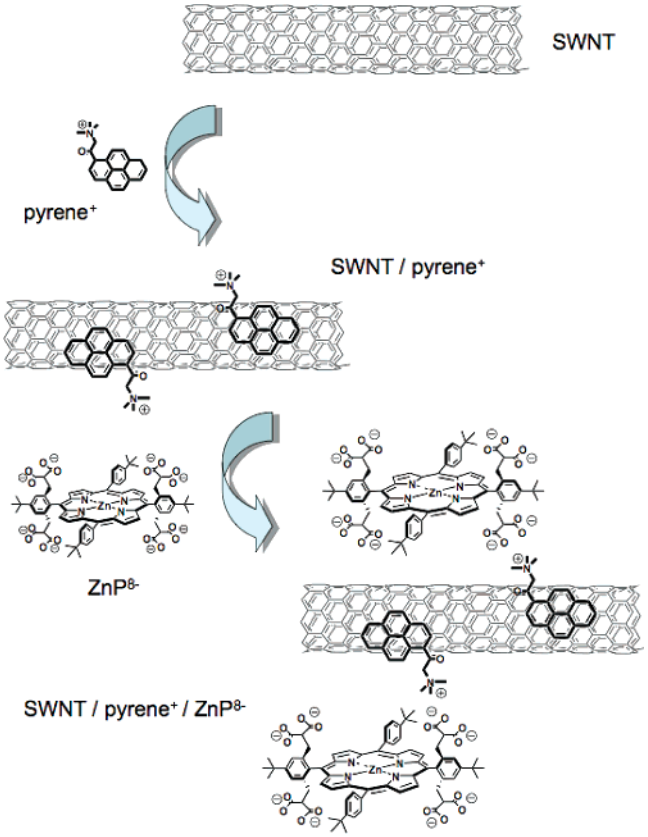

Results and Discussion

Pyrene. The absorption spectrum of **pyrene**$^{+}$ in a buffered aqueous solution deviates substantially from the well-known and well-studied features of pyrene in organic solvents.[8] In particular, a series of rather broad absorption bands that center around 285, 365, and 395 nm characterizes the yellowish solution of **pyrene**$^{+}$. In comparison, the longest wavelength transition of pyrene in organic solvents appears as a sharp maximum at 340 nm. To dissect the influence that substitution, solvent polarity, or electronic effects might have on the transitions in **pyrene**$^{+}$, we complemented our measurements with similar data on a colorless sample of pyrene−methanol that exhibits solubility in nonpolar and polar solvents.[9] In this case, the features seen are comparable to those of pyrene (i.e.,

(2) (a) Imahori, H.; Sakata, Y. *Adv. Mater*. **1997**, *9*, 537. (b) Prato, M. *J. Mater. Chem*. **1997**, *7*, 1097. (c) Martín, N.; Sánchez, L.; Illescas, B.; Pérez, I. *Chem. Rev*. **1998**, *98*, 2527. (d) Diederich, F.; Gomez-Lopez, M. *Chem. Soc. Rev*. **1999**, *28*, 263. (e) Guldi, D. M.; Prato, M. *Acc. Chem. Res.* **2000**, *33*, 695. (f) Gust, D.; Moore, T. A.; Moore, A. L. *Acc. Chem. Res.* **2001**, *34*, 40. (g) Guldi, D. M.; Prato, M. *Chem. Commun*. **2004**, 2517. (h) Guldi, D. M. *Chem. Soc. Rev*. **2002**, *31*, 22. (i) Guldi, D. M.; Rahman, G. M. A.; Sgobba, V.; Kotov, N. A.; Bonifazi, D.; Prato, M. *J. Am. Chem. Soc*. **2006**, *128*, 2315. (j) Mihaela, B.; Pedro, G. R. *J. Nanosci. Nanotechnol*. **2006**, *6*, 289. (k) Wu, W.; Zhang, S.; Li, Y.; Li, J.; Liu, L.; Qin, Y.; Guo, Z.-X.; Dai, L.; Ye, C.; Zhu, D. *Macromolecules* **2003**, *36*, 6286. (l) Lee, J. U. *Appl. Phys. Lett*. **2005**, *87*, 073101/1. (m) Jin, M. H.-C.; Dai, L. *Opt. Sci. Eng*. **2005**, *99*, 579.

(3) (a) Guldi, D. M.; Marcaccio, M.; Paolucci, D.; Paolucci, F.; Tagmatarchis, N.; Tasis, D.; Vazquez, E.; Prato, M. *Angew. Chem., Int. Ed*. **2003**, *42*, 4206. (b) Alvaro, M.; Atienzar, P.; de la Cruz, P.; Delgado, J. L.; Garcia, H.; Langa, F.; *J. Phys. Chem. B* **2004**, *108*, 12691.

(4) (a) Li, H.; Martin, R. B.; Harruff, B. A.; Carino, R. A.; Allard, L. F.; Sun, Y.-P. *Adv. Mater*. **2004**, *16*, 896. (b) Baskaran, D.; Ways, J. W.; Zhang, X. P.; Bratcher, M. S. *J. Am. Chem. Soc.* **2005**, *127*, 6916.

(5) (a) Murakami, H.; Nomura, T.; Nakashima, N. *Chem. Phys. Lett*. **2003**, *378*, 481. (b) Chen, J.; Collier, C. P. *J. Phys. Chem. B* **2005**, *109*, 7605. (c) Li, H.; Zhou, B.; Lin, Y.; Gu, L.; Wang, W.; Fernando, K. A. S.; Kumar, S.; Allard, L. F.; Sun, Y.-P. *J. Am. Chem. Soc*. **2004**, *126*, 1014. (d) Hasobe, T.; Fukuzumi, S.; Kamat, P. V. *J. Am. Chem. Soc.* **2005**, *127*, 11884. (e) Nakashima, N.; Tomonari, Y.; Murakami, H. *Chem. Lett*. **2002**, 638. (f) Chen, R. J.; Zhang, Y.; Wang, D.; Dai, H. *J. Am. Chem. Soc*. **2001**, *123*, 3838.

(6) (a) Guldi, D. M.; Taieb, H.; Rahman, G. M. A.; Tagmatarchis, N.; Prato, M. *Adv. Mater*. **2005**, *17*, 871. (b) Guldi, D. M.; Rahman, G. M. A.; Jux, N.; Tagmatarchis, N.; Prato, M. *Angew. Chem., Int. Ed*. **2004**, *43*, 5526. (c) Guldi, D. M.; Rahman, G. M. A.; Jux, N.; Balbinot, D.; Tagmatarchis, N.; Prato, M. *Chem. Commun*. **2005**, 2038. (d) Guldi, D. M.; Rahman, G. M. A.; Jux, N.; Balbinot, D.; Hartnagel, U.; Tagmatarchis, N.; Prato, M. *J. Am. Chem. Soc.* **2005**, *127*, 9830. (e) Guldi, D. M.; Rahman, G. M. A.; Ramey, J.; Marcaccio, M.; Paolucci, D.; Paolucci, F.; Qin, S. H.; Ford, W. T.; Balbinot, D.; Jux, N.; Tagmatarchis, N.; Prato, M. *Chem. Commun*. **2004**, 2034. (f) Rahman, G. M. A.; Guldi, D. M.; Campielli, S.; Prato, M. *J. Mater. Chem*. **2006**, *16*, 62.

(7) (a) Guldi, D. M.; Rahman, G. M. A.; Jux, N.; Prato, M.; Qin, S.; Ford, W. T. *Angew. Chem., Int. Ed*. **2005**, *44*, 2015. (b) Guldi, D. M. *J. Phys. Chem. B* **2005**, *109*, 11432. (c) Guldi, D. M.; Rahman, G. M. A.; Zerbetto, F.; Prato, M. *Acc. Chem. Res*. **2005**, *38*, 871. (d) Kymakis, E.; Amaratunga, G. A. J. *Sol. Energy Mater. Sol. Cells* **2003**, *80*, 465.

(8) (a) Turro, N. J. *Modern Molecular Photochemistry*; University Science Books Press: Menlo Park, CA, 1978. (b) Khakhel, O. A. *J. Appl. Spectrosc*. **2001**, *68*, 280. (c) Yoshihara, K.; Kasuya, T.; Inoue, A.; Nagakura, S. *Chem. Phys. Lett*. **1971**, *9*, 469. (d) Winnik, F. M. *Chem. Rev*. **1993**, *93*, 587. (e) Barashkov, N. N.; Sakhno, T. V.; Nurmukhametov, R. N.; Khakhel, O. A. *Polymer* **1996**, *37*, 1109. (f) Haynes, D. R.; Nishimura, A. M.; Gorge, S. M. *Chem. Phys. Lett*. **1989**, *159*, 599. (g) Marconi, G.; Salvi, P. R. *Chem. Phys. Lett*. **1986**, *123*, 254. (h) Slifkin, M. A.; Al-Chalabi, A. O. *Chem. Phys. Lett*. **1975**, *31*, 198.

(9) Guldi, D. M.; Menna, E.; Maggini, M.; Marcaccio, M.; Paolucci, D.; Paolucci, F.; Campidelli, S.; Prato, M.; Rahman, G. M. A.; Schergna, S. *Chem.—Eur. J.* **2006**, *12*, 3975.

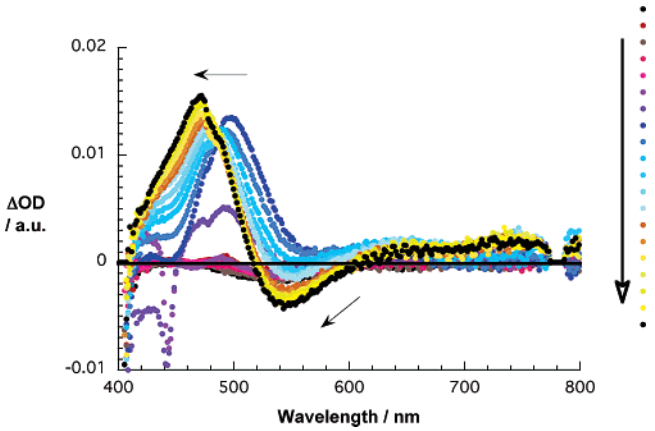

Figure 1. Differential absorption spectra (visible) obtained upon femtosecond flash photolysis (387 nm) of **pyrene**$^+$ in nitrogen saturated aqueous solutions with several time delays between 0 and 5 ps at room temperature. Arrows indicate the evolution of differential changes.

sharp maxima at 345 nm). The spectra of **pyrene**$^+$ in several different alcohols or THF remain virtually unchanged. At first glance, we must conclude that the effects are mainly electronic and originate from the strongly electronic withdrawing nature of the trimethylammonium acetyl functionality. Still we cannot discard a different alternative, namely, aggregation that is driven by the amphilic nature of **pyrene**$^+$. This argument is applicable for both polar and nonpolar media due to the formation of micellar and inverse micellar architecture of aggregates. Remarkably, concentrations as low as 10^{-7} M led quantitatively to the same effects. In other words, if in fact aggregation plays a measurable role for **pyrene**$^+$, then its overall critical micellar concentrations would set in at very low concentrations.

Also, when pyrene, pyrene−methanol, and **pyrene**$^+$ are compared in fluorescence measurements substantial differences arise (Figure S1, Supporting Information). The structured emission of pyrene with the lowest energy band, ~410 nm, is substituted in **pyrene**$^+$ by a broadly shaped maximum at 500 nm with a tail around 400 nm on the high-energetic side and around 600 nm on the low-energetic side. A fluorescence quantum yield of 0.01 was measured. The fine structure that governs the fluorescing transitions from the different vibrational levels of pyrene and pyrene−methanol is largely missing. Notably, around 385 nm, the Raman peak of water is seen, which dominates the fluorescence spectrum in this region. The picture is somewhat reminiscent of the exciplex emission seen for pyrene, though our experiments do not support the notion of the formation of excited-state dimers (i.e., down to concentrations of 10^{-8} M).

In time-resolved fluorescence measurements, the **pyrene**$^+$ emission at 500 nm was studied in parallel with the fluorescence decay of pyrene−methanol. While for pyrene−methanol in aerated THF a respectable lifetime of 109 ± 5 ns was found, comparable to that of pyrene, the fluorescence of **pyrene**$^+$ is relatively short-lived (i.e., 2.7 ± 0.5 and 13.5 ± 2.0 ns in water and in THF, respectively).

Figure 1 illustrates the differential absorption changes that occur in less than a picosecond following 150 fs excitation at 387 nm of **pyrene**$^+$. A stable transient maximum develops at 475 nm as a consequence of the blue shifting of a very short-lived transient that initially has a maximum at 500 nm. The 475 nm maximum is flanked by fluorescence-stimulated bleaching between 500 and 600 nm. The analyses of the kinetics at several wavelengths, in the range of the maximum and that of the bleaching, helps to link decay and formation and to derive a rate constant for forming the stable **pyrene**$^+$ excited state as 9.1×10^{11} s^{-1}. Mechanistically, the process is proposed to relate to a downward conversion of an upper electronically excited state to the lowest vibrational level of the **pyrene**$^+$ singlet excited state. The singlet excited state is stable on the time scale of our femtosecond experiments (i.e., up to 1.5 ns).

The singlet excited-state energy of **pyrene**$^+$ is derived from the energy average of the longest wavelength absorption and the shortest wavelength fluorescence as 2.7 eV. Of relevance for charge separation processes, notice that in electrochemical experiments (vide infra and Figure 7), the oxidation potential of **pyrene**$^+$ is +1.3 V (vs SCE).

Porphyrin. The absorptions of **MP**$^{8-}$ (M = Zn or H_2, see Scheme 1) in buffered aqueous solutions are virtually identical to those of their simpler tetraphenyl porphyrin precursors (i.e., ZnP or H_2P) in organic media. **ZnP**$^{8-}$ and **H$_2$P**$^{8-}$ exhibit high-energy and strong Soret transitions (S_0-S_2) at 426 and 418 nm, respectively. In the low-energy range, Q-bands (S_0-S_1) for **ZnP**$^{8-}$ occur at 560 and 600 nm and for **H$_2$P**$^{8-}$ at 470, 518, 550, and 588 nm. Notably, the **H$_2$P**$^{8-}$ transitions are lower in energy than the **ZnP**$^{8-}$ ones.

The steady-state fluorescence spectra are exact mirror images of the absorption spectra (not shown). For **ZnP**$^{8-}$, the maximum fluorescence appears at 612 and 665 nm, while **H$_2$P**$^{8-}$ fluoresces at 658 and 715 nm. The shifts in excited-state energy are not the only differences seen between the excited-state features of the two porphyrins. Also their fluorescence quantum yields and fluorescence lifetimes differ notably with values of 0.04 and 2.1 ns (**ZnP**$^{8-}$) and 0.11 and 9.4 ns (**H$_2$P**$^{8-}$).

To characterize the differential absorption changes associated with the formation and decay of **MP**$^{8-}$ singlet excited states, we pumped light into their singlet ground states with femtosecond laser pulses at 387 nm. Transient maxima at 640 nm (**ZnP**$^{8-}$) and 670 nm (**H$_2$P**$^{8-}$), together with transient bleaching at 568 nm (**ZnP**$^{8-}$) and 520 nm (**H$_2$P**$^{8-}$) were observed (Figure 2). Important here is that the singlet lifetimes quantitatively match the fluorescence lifetimes: **ZnP**$^{8-}$ = 2.3 ± 0.2 ns and **H$_2$P**$^{8-}$ = 10.2 ± 0.5 ns. Both singlet excited states convert, similar to their tetraphenylporphyrin analogues in organic solvent environments, via an efficient intersystem crossing to the energetically lower lying triplet excited states.[6b,10] Indeed, in complementary nanosecond experiments, triplet fingerprints (Figure S2, Supporting Information) are established in the near-infrared with maxima for **ZnP**$^{8-}$ at 860 nm and for **H$_2$P**$^{8-}$ at 780 nm. The triplets are metastable and decay in an oxygen-free environment on the longer nano- or microsecond time scale with unimolecular dynamics. Energetically, we place the **ZnP**$^{8-}$ and **H$_2$P**$^{8-}$ triplets at 1.53 and 1.40 eV, respectively.[11]

SWNT−Poly(sodium 4-styrenesulfonate) (PSS). As a SWNT model system for our studies, we wanted to avoid the use of pristine SWNTs, which are insoluble and indispersible. Therefore, we decided to use SWNTs that are grafted with poly(sodium 4-styrenesulfonate) (**SWNT−PSS**$^{n-}$), containing 55/

(10) (a) Gartz, H.; Penzkofer, A. *Chem. Phys.* **2000**, *254*, 363. (b) Nawakowska, M.; Sterzel, M.; Zapotoczny, S. *Photochem. Photobiol.* **2005**, *81*, 1227. (c) Fukuzumi, S.; Hasobe, T.; Ohkubo, K.; Crossley, M. J.; Kamat, P. V.; Imahori, H. *J. Porphyrins Phthalocyanines* **2004**, *8*, 191.

(11) Our energetic estimation is based on assuming energetic comparability with tetraphenyl porphyrin.

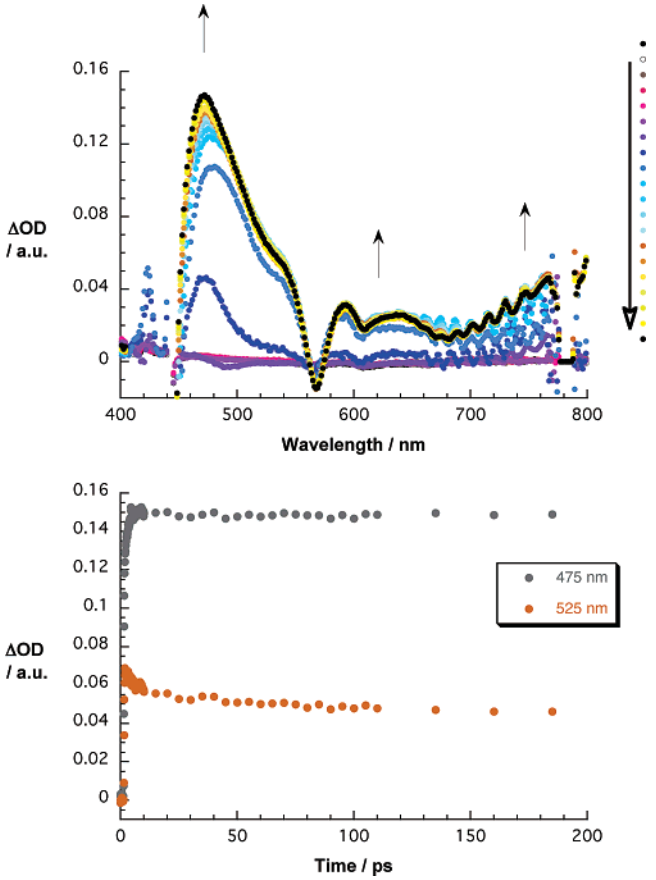

Figure 2. Differential absorption spectra (top; visible) obtained upon femtosecond flash photolysis (387 nm) of **ZnP**$^{8-}$ in nitrogen-saturated aqueous solutions with several time delays between 0 and 5 ps at room temperature (arrows indicate the evolution of differential changes) and time-absorption profiles (bottom) of the spectra shown above at 475 and 525 nm, monitoring the decay of the porphyrin singlet excited state.

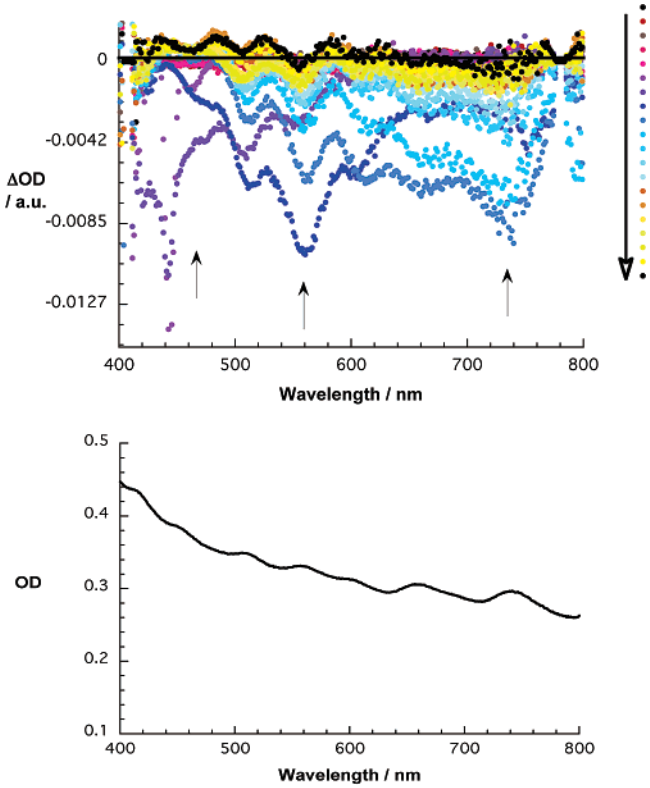

Figure 3. Differential absorption spectra (top; visible) obtained upon femtosecond flash photolysis (387 nm) of **SWNT**−**PSS**$^{n-}$ in nitrogen-saturated aqueous solutions with several time delays between 0 and 5 ps at room temperature (arrows indicate the evolution of differential changes) and absorption spectrum (bottom) of **SWNT**−**PSS**$^{n-}$.

45 SWNT/PSS by weight.[6e,12] These relatively soluble SWNTs are not too heavily functionalized, so they maintain most of the original electronic properties. As a matter of fact, the cathodic voltammetric curve of a **SWNT**−**PSS**$^{n-}$ aqueous solution closely resembles that of **SWNT/pyrene**$^{+}$ hybrids (vide infra and Figure 7) thus highlighting very similar electron-accepting properties of the above model system to those of pristine **SWNT**. In the absorption spectra of **SWNT**−**PSS**$^{n-}$, the characteristic van Hove transitions of semiconducting SWNTs are discernible throughout the UV−vis−NIR region. More precisely, they appear in the 600−900 and 1000−1500 nm regions, while those of metallic SWNTs show their transitions in the 500−600 nm range.[13]

When an aqueous dispersion of **SWNT**−**PSS**$^{n-}$ is photoexcited with short 387 nm laser pulses, differential absorption changes are registered in the 400−800 nm range that are dominated by transient bleach of what seems to be reminiscent of the ground-state absorptions. More precisely, we see a mirror image of the characteristic van Hove transitions. To demonstrate this, the absorption spectrum in Figure 3 is compared with the differential absorption spectrum. Interestingly, the transient bleach is very short-lived (i.e., ∼1 ps), and its lifetime depends strongly on the wavelength: transitions in the blue are typically shorter lived than those in the red.

Pyrene/Porphyrin. To test **pyrene**$^{+}$/**MP**$^{8-}$ interactions, dilute aqueous solution of **ZnP**$^{8-}$ and **H$_2$P**$^{8-}$ were titrated with variable amounts of **pyrene**$^{+}$ to form **pyrene**$^{+}$/**ZnP**$^{8-}$ and **pyrene**$^{+}$/**H$_2$P**$^{8-}$, respectively. A typical example for an absorption spectroscopic assay is given in Figure S3. Relative to the component spectra (i.e., **pyrene**$^{+}$, **ZnP**$^{8-}$, and **H$_2$P**$^{8-}$), two spectral developments should be emphasized. First, the **MP**$^{8-}$ transitions, Soret and Q-bands, shift incrementally to the red. The Soret bands show typically the biggest changes with shifts of up to 3 nm. Second, the presence of isosbestic points at 428 nm (i.e., **ZnP**$^{8-}$) and at 418 nm (i.e., **H$_2$P**$^{8-}$) speak for the clean transformations of **MP**$^{8-}$ (i.e., start point of the titration) into **pyrene**$^{+}$/**MP**$^{8-}$ (i.e., end point of the titration).

When **MP**$^{8-}$ was added, the **pyrene**$^{+}$ fluorescence also underwent several key changes. Figure S4 of the Supporting Information summarizes the steady-state fluorescence with 367 nm excitation. First, the **pyrene**$^{+}$ fluorescence intensities decrease exponentially and converge to a final plateau. Second, the intensity of the **MP**$^{8-}$ fluorescence peaks grow-in simultaneously at 612 and 665 nm (**ZnP**$^{8-}$) or at 658 and 715 nm (**H$_2$P**$^{8-}$). Third, the **pyrene**$^{+}$ fluorescence lifetime (i.e., 2.7 ns), which in the absence of **MP**$^{8-}$ is best fitted by a monoexponential rate law, is replaced by a biexponential decay with a long-lived (2.7 ns) and a short-lived component (<0.1 ns). Due to electrostatic attraction between the negatively charged **MP**$^{8-}$ and the cationic **pyrene**$^{+}$, stable **pyrene**$^{+}$/**MP**$^{8-}$ ensembles are formed. The synopsis of the emission studies is an efficient transduction of excited-state energy of the **pyrene**$^{+}$

(12) (a) Qin, S.; Qin, D.; Ford, W. T.; Zhang, Y.; Kotov, N. A. *Chem. Mater.* **2005**, *17*, 2131. (b) Qin, S.; Qin, D.; Ford, W. T.; Resasco, D. E.; Herrera, J. E. *Macromolecules* **2004**, *37*, 3965.
(13) We did not test them up to this point in any fluorescence experiments.

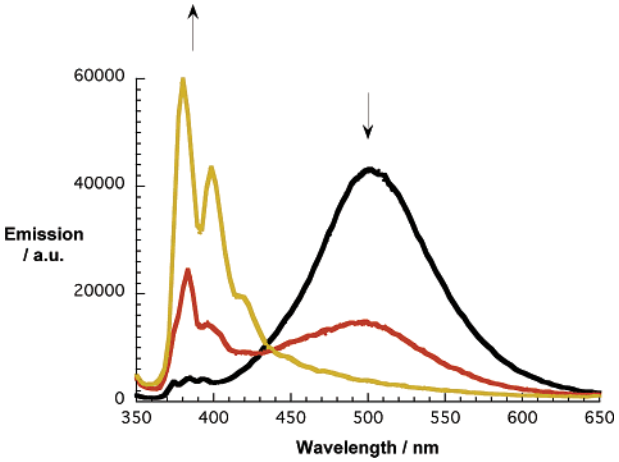

Figure 4. Fluorescence spectra of **SWNT/pyrene**$^+$ in aqueous solutions at pH 6.5 after several cycles (see Experimental Section for details) of removing free **pyrene**$^+$. The corresponding absorption spectra are shown in Figure S6, Supporting Information. Black, red, and beige spectra correspond to increasing number of removal cycles.

singlet (2.7 eV) to those of **ZnP**$^{8-}$ (2.1 eV) and **H$_2$P**$^{8-}$ (1.9 eV).[14,15]

On the other hand, when the **MP**$^{8-}$ transitions are irradiated, only a moderate fluorescence quenching evolves. Based on a quenching efficiency of less than 15% under conditions where the **pyrene**$^+$ fluorescence is quantitatively quenched, we conclude that deactivation of the photoexcited porphyrins through either energy or electron transfer should be excluded. A thermodynamic evaluation leads to the same conclusion; that is, both processes would be highly endothermic. Singlet−singlet energy transfer would be uphill by about 0.5 eV, and the driving force for charge separation would be $+0.7 \pm 0.1$ eV.[16]

Competitive light absorption of the **pyrene**$^+$ and **ZnP**$^{8-}$ chromophores appears as the only feasible rationale to explain the 15% quenching in the steady-state experiments. To substantiate this assumption, the same samples were investigated in time-resolved fluorescence decay measurements. Close inspection of the 610 and 665 nm fluorescence profiles, as representative decays for **ZnP**$^{8-}$ and **H$_2$P**$^{8-}$, respectively, reveals nearly unchanged lifetimes of 2.1 ± 0.2 and 9.4 ± 0.5 ns throughout the titration assays. This confirms the lack of excited-state interactions that evolve from photoexciting **MP**$^{8-}$ in **pyrene**$^+$/**MP**$^{8-}$.

Additional evidence that supports the lack of electron donor−acceptor interactions comes from transient absorption measurements. The spectral features and decay/formation dynamics associated with **MP**$^{8-}$ are in **pyrene**$^+$/**MP**$^{8-}$ strictly superimposable with those that are gathered for the **ZnP**$^{8-}$ and **H$_2$P**$^{8-}$ building blocks (vide supra).

SWNT/Pyrene. When the absorption spectra of an aqueous **SWNT/pyrene**$^+$ solution with that of bare **pyrene**$^+$ are compared, several key differences are seen (see Figure S5, Supporting Information). First, the $\pi-\pi$ transitions of **pyrene**$^+$ are slightly red-shifted (i.e., about 1 nm). Second, the overall absorption cross-section increases, particularly in the vis and NIR regions. Third, the characteristic van Hove transitions of SWNT are discernible in the vis−NIR region up to around 450 nm, where the $\pi-\pi^*$ transition of **pyrene**$^+$ dominate the spectrum. In fact, a D_2O spectrum of **SWNT/pyrene**$^+$ verifies that the van Hove transitions extend all the way out to 1500 nm and that they track those seen for a DMF-sonicated suspension of SWNTs.[6b] Collectively, these observations confirm the presence of both solubilized SWNTs and **pyrene**$^+$.

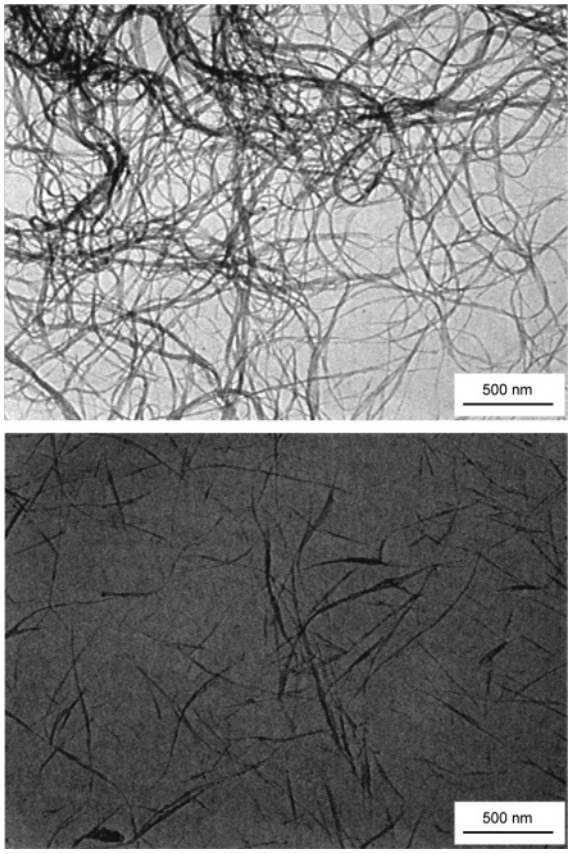

Figure 5. TEM images of **SWNT** (top) and of **SWNT/pyrene**$^+$ (bottom).

Decisive evidence for **SWNT/pyrene**$^+$ interactions came from emission experiments, which showed quenching of the **pyrene**$^+$ fluorescence (i.e., 500 nm) that is as large as 70%. However, Figure 4 reveals two major components for the **pyrene**$^+$ fluorescence when **SWNT** are present. As already mentioned the broad visible fluorescence that lacks any particular fine structure is one component. In addition, the near-visible region shows the typical fine structure known for **pyrene** as a second component. This led us to perform two additional workup cycles, namely, centrifugations and resuspensions (i.e., in water) with the objective to remove excess **pyrene**$^+$. Figure 4 demonstrates the corresponding fluorescence spectra following photoexcitation at 340 nm. Most interestingly, we see the systematic amplification of the near-visible fluorescence, while the visible fluorescence diminishes synchronously. Although we cannot determine the exact **pyrene**$^+$ concentration, due to the dominance of the SWNT transitions, they are comparable to those mentioned in the preceding section on **pyrene**$^+$ ($\sim 10^{-7}$ M). In summary, $\pi-\pi$ interactions between **SWNT** and

(14) The quantum yields were determined by the comparative method.

(15) When the exponential I/I_0 versus **MP**$^{8-}$ concentration titration curve was fit to $I = I_0 + \Delta I/(2S_0)[K_{diss} + X + S_0 - \sqrt{(K_{diss}+X+S_0)^2 - 4XS_0}]$, values between 10^4 and 10^5 M^{-1} were obtained for the association constant of the supramolecular **pyrene**$^+$/**MP**$^{8-}$ complexes at pH 7.2. I, I_0, and ΔI ($\Delta I = I_0 - I$) are the fluorescence intensities observed at 500 nm, $K_{diss} = 1/K_{ass}$, and X and S_0 are the titrant (**MP**$^{8-}$) and substrate (**pyrene**$^+$) concentrations, respectively.

(16) Oxidation of **pyrene**$^+$ is located at +1.3 V and reduction of **ZnP**$^{8-}$ is at −1.42 V versus SCE.

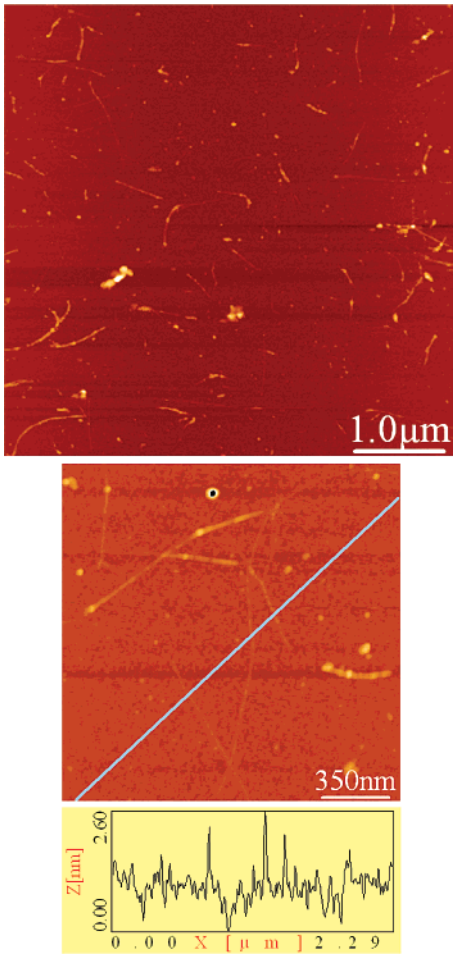

Figure 6. AFM images of **SWNT/pyrene**$^+$ nanohybrid on silicon wafer: general view of the very thin bundles and individual tubes in the top image; close up and diameter of a single nanotube in the bottom image.

pyrene$^+$ breaks up individual clusters of the components and yields nearly isolated **SWNT/pyrene**$^+$ hybrids.

In time-resolved fluorescence only a long-lived component (i.e., 2.6 ns) is discernible, which matches that measured for just **pyrene**$^+$. Consequently, as a likely explanation for this observation we must assume to have measured the fluorescence of free and not SWNT-immobilized **pyrene**$^+$. Photoexcited **pyrene**$^+$ immobilized onto SWNTs should deactivate within a time frame faster than the time resolution of our apparatus (i.e., 100 ps).

Indirect evidence for **SWNT/pyrene**$^+$ interactions stem from transmission electron microscopy (TEM) and atomic force microscopy (AFM). Both techniques assist in the visualization of SWNT.[2i,6b] Inspecting the TEM images of pristine **SWNT** shows the presence of large aggregates of nanotubes. These micrometer objects resemble wool balls. In the case of **SWNT/pyrene**$^+$, well dispersed small bundles are distinguished (Figure 5). For the AFM studies, the samples were prepared by spin coating. This technique allows the almost complete dispersion of **SWNT/pyrene**$^+$ onto the surface. Most importantly, very thin bundles of **SWNT/pyrene**$^+$, 1−3 μm in length and 3−20 nm in diameter, and individual **SWNT/pyrene**$^+$ with diameters as small as 1.3 nm are discernible (Figure 6). **Pyrene**$^+$ acts as a surfactant; it slowly interferes with the $\pi-\pi$ interactions between **SWNT** and allows the debundling and the solubilization of **SWNT**.

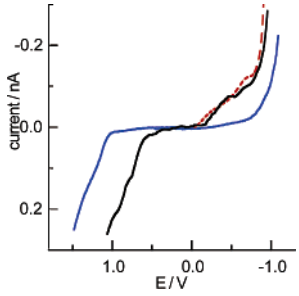

Figure 7. Steady-state voltammetric curves of **pyrene**$^+$ (blue line) and **SWNT/pyrene**$^+$ (black line) aqueous solutions in the absence of any supporting electrolyte. Red (dashed) line is the steady-state voltammetric curve (current × 10^{-1}) of **SWNT**−**PSS**^{n}$^-$ in 0.01 M Na_2SO_4 aqueous solution. Scan rate = 0.05 Vs^{-1}; working electrode is a Pt disk (5 μm radius). Potentials are referenced to SCE.

Steady-state voltammetric experiments were carried out in aqueous solutions of either **pyrene**$^+$ or **SWNT/pyrene**$^+$, in the absence of any supporting electrolyte, that is, under conditions similar to the photophysical experiments (Figure 7).

Importantly, avoiding the addition of supporting electrolyte was found necessary because severe flocculation of both solutions and subsequent precipitation of either **pyrene**$^+$ or **SWNT/pyrene**$^+$ were otherwise observed (upon addition of $LiClO_4$ or Na_2SO_4). Because of the ensuing large solution resistance, the voltammetric experiments were carried out using a Pt disk ultramicroelectrode (5 μm radius) and, under steady-state conditions, obtained with low potential scan rates ($\leq$0.05 V/s). In the rather narrow potential window allowed by water, the voltammetric curve of the **pyrene**$^+$ solution only displays the one-electron oxidation of **pyrene**$^+$ (Figure 7, blue trace) with a half-wave potential of +1.3 V. No appreciable reduction wave was observed in the negative potentials region. Conversely, the voltammetric curve of **SWNT/pyrene**$^+$ showed (Figure 7, black trace) both anodic and cathodic processes. The onset of the cathodic wave was located at around −0.15 V, while that of the anodic one was at around +0.6 V. Such waves were attributed to the reduction and oxidation of SWNTs, respectively. Notably, the above potential values are in very good agreement with those previously found for **SWNT**−**PSS**^{n}$^-$ (whose cathodic curve is also shown, for the sake of comparison, in Figure 7) or pyrrolidine-functionalized SWNT solutions[6e] and also agree with those obtained by quantum chemical simulations.[17] Interestingly, the anodic wave in the CV curve of **SWNT/pyrene**$^+$ suggests the superimposition of two distinct processes; the process occurring at more positive potentials is located at about +0.9 V. Since no such process was previously found in the voltammetric curves of other soluble SWNTs, we assume that the anodic wave at +0.9 V is associated with the oxidation of the **pyrene**$^+$ moieties in **SWNT/pyrene**$^+$ nanohybrids. The rather large potential shift of 0.4 V observed with respect to free **pyrene**$^+$ (1.3 V) would then result from the electronic interaction between the two π-systems that renders the oxidation of **pyrene**$^+$ moieties so much easier.[9]

Decisive information about excited-state interactions came from transient absorption measurements. Figure 8 gathers transient absorption spectra recorded upon 387 nm excitation

(17) (a) Hu, Y.; Sinnott, S. B. *J. Mater. Chem.* **2004**, *14*, 719. (b) Yang, M.; Koutsos, V.; Zaiser, M. *J. Phys. Chem. B* **2005**, *109*, 10009. (c) Melle-Franco, M.; Marcaccio, M.; Paolucci, D.; Paolucci, F.; Georgakilas, V.; Guldi, D. M.; Prato, M.; Zerbetto, F. *J. Am. Chem. Soc.* **2004**, *126*, 1646.

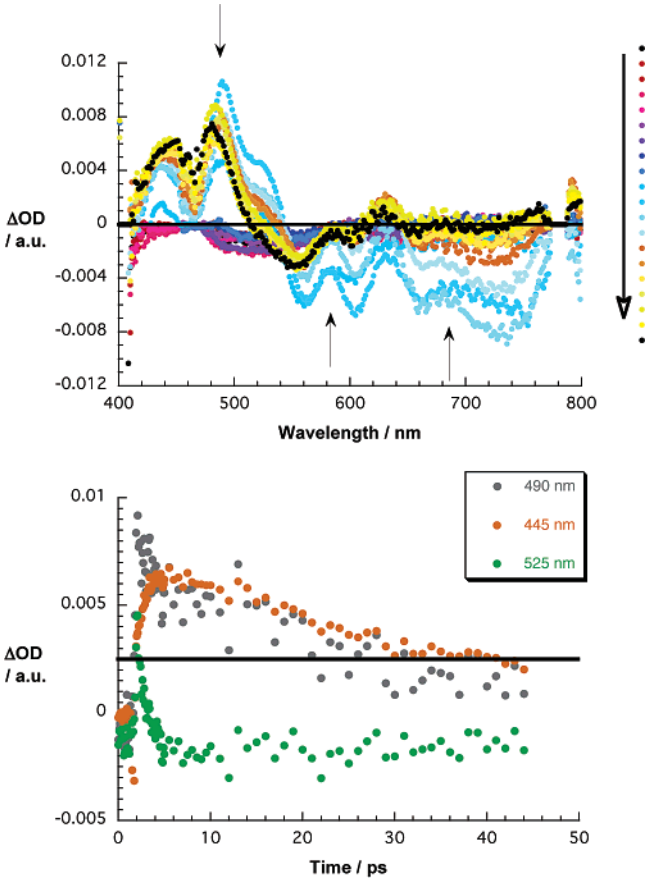

Figure 8. Differential absorption spectra (top; visible) obtained upon femtosecond flash photolysis (387 nm) of **SWNT/pyrene**$^+$ in nitrogen-saturated aqueous solutions with several time delays between 0 and 5 ps at room temperature (arrows indicate the evolution of differential changes) and time-absorption profiles (bottom) of the spectra shown above at 445, 490, and 525 nm.

of **SWNT/pyrene**$^+$. When comparing Figure 8 with Figures 1 and 4, we conclude that changes in the 400−600 nm region reflect mainly features associated with **pyrene**$^+$ excited state, while changes in the 600−800 nm region correspond to SWNT. Importantly, **pyrene**$^+$ decays with ultrafast dynamics of 6.6×10^{11} s^{-1}.

In complementary TGA measurements (see Figure S7, Supporting Information), the loss of weight for **SWNT/pyrene**$^+$ is 17% at 600 °C, while **SWNT** under the same experimental conditions give rise to only a loss of weight of about 7%. Consequently, we extrapolate 10% of pyrene, which corresponds to a ratio of 1 to 280 carbon atoms.

SWNT/Pyrene/Porphyrin. Convenient and informative tests on the association of **MP**$^{8-}$ with **SWNT/pyrene**$^+$, for which a sketch is illustrated in Scheme 1, included titration experiments that examined spectral changes both in fluorescence and in absorption.

Absorption measurements linked to the formation of **SWNT/pyrene**$^+$**/MP**$^{8-}$ are essentially identical to what has been noted in the absence of SWNT, that is, for interacting **pyrene**$^+$ with **MP**$^{8-}$, vide supra. For example, dilute aqueous solutions of **MP**$^{8-}$ were titrated with variable concentrations of **SWNT/pyrene**$^+$, and a clean conversion from free **MP**$^{8-}$ to **SWNT/pyrene**$^+$**/MP**$^{8-}$ is substantiated through isosbestic points and red shift of the Soret and Q-bands. Interestingly, the **pyrene**$^+$ $\pi-\pi$ transitions are subjected to an additional red shift of 2 nm, which indicates that **SWNT/pyrene**$^+$ and **MP**$^{8-}$ interact electrostatically.

The additions of **SWNT/pyrene**$^+$ to **MP**$^{8-}$ were followed using 430 nm as the excitation wavelength, where the isosbestic point was observed in the absorption spectrum. Under these conditions, competitive light absorption by **SWNT/pyrene**$^+$ is minimal. When **SWNT/pyrene**$^+$ is present the fluorescence emission intensity decreased.[6b] The decrease is exponential and depends solely on the **SWNT/pyrene**$^+$ concentration. Inspection of this figure reveals that simultaneous with the quenching of the **ZnP**$^{8-}$ or **H$_2$P**$^{8-}$ emission, new lower-energy emission bands develop.

In **SWNT/pyrene**$^+$**/ZnP**$^{8-}$, the **MP**$^{8-}$ fluorescence profiles were now best fitted by lifetimes of 2.1 ± 0.2 and 0.2 ± 0.05 ns. The two lifetimes are maintained throughout the titration assay. As the concentration of **SWNT/pyrene**$^+$ increases, the contribution of the short-lived component increases as well. In such mixtures, intrahybrid **SWNT/MP**$^{8-}$ interactions are therefore responsible for one kinetic component (i.e., the fast one) and regular **MP**$^{8-}$ excited-state deactivations give rise to the other component (i.e., the slow one). At all concentrations, the pre-exponential factors give rise to good agreement with the distribution of emitting species, that is, bound, immobilized versus free, nonimmobilized **ZnP**$^{8-}$ or **H$_2$P**$^{8-}$.

Upon addition of acid to adjust the pH to around 5, the original long-lived fluorescence component of **ZnP**$^{8-}$ or **H$_2$P**$^{8-}$ is restored and, at the same time, the short-lived species disappears. This demonstrates that the **SWNT/pyrene**$^+$**/MP**$^{8-}$ complex formation is reversible. All the data therefore point toward a static quenching event occurring inside well-defined hybrids of **SWNT/pyrene**$^+$**/ZnP**$^{8-}$ and **SWNT/pyrene**$^+$**/H$_2$P**$^{8-}$. The most likely excited-state quenching process involves electron transfer; that is, the oxidation of porphyrin ($E_{1/2} = 0.77$ V) and the reduction of SWNT ($E_{1/2} = -0.15$ V), with a corresponding favorable driving force of 0.92 V.

Finally, **SWNT/pyrene**$^+$**/ZnP**$^{8-}$ was tested in transient absorption measurements. Please note that at the 387 nm excitation, **ZnP**$^{8-}$ is the most strongly absorbing entity. In line with this, detecting the instantaneous growth of the broad absorption between 570 and 750 nm confirms the successful **ZnP**$^{8-}$ excitation in **SWNT/pyrene**$^+$**/ZnP**$^{8-}$. However, instead of seeing the slow intersystem crossing (ISC) dynamics (4.0×10^8 s^{-1}, see Figure 3) that **ZnP**$^{8-}$ exhibits, the singlet−singlet absorption in the presence of **SWNT/pyrene**$^+$ decays with accelerated, ultrafast dynamics (6.3×10^9 s^{-1}, see Figure 9). This value is in satisfactory agreement with the time-resolved fluorescence experiments. Spectroscopically, the transient absorption changes, taken after the completion of the decay, bear no resemblance to the **ZnP**$^{8-}$ triplet excited state. Spectroscopic features of the new intermediate in the 400−800 nm range are governed by broad absorptions between 600 and 800 nm, indicating **ZnP**$^{8-}$ centered redox products.[6b]

It is concluded that an energetically low-lying radical ion pair is formed as a product of an ultrafast photoinduced electron transfer. Figure 10 exemplifies the spectral changes seen in the case of **SWNT/pyrene**$^+$**/ZnP**$^{8-}$. The **ZnP**$^{8-}$ radical cation spectroscopic fingerprints were employed as reliable probes to determine the lifetime of the associated radical ion pair state. The decay curves were well fitted by a single exponential decay

Table 1. Summary of the Photophysical and Electrochemical Data

	species										
	SWNT/pyrene$^+$/ H_2P^{8-}	**SWNT/pyrene$^+$/ ZnP^{8-}**	**SWNT/ pyrene$^+$**	**pyrene$^+$/ H_2P^{8-}**	**pyrene$^+$/ ZnP^{8-}**	**SWNT–PSS^{n-}**	**H_2P^{8-}**	**ZnP^{8-}**	**pyrene$^+$**	pyrene–methanol	pyrene
abs. (nm)	further red shift for **pyrene**$^+$ by 2 nm	further red shift for **pyrene**$^+$ by 2 nm	red shift for **pyrene**$^+$ by 1−2 nm	red shift by 3 nm for **H_2P^{8-}**; isosbestic points at 418	red shift by 3 nm for **ZnP^{8-}**; isosbestic points at 428	600−900 and 1000−1500 (semiconducting NT); 500−600 (metallic NT)	423, 470, 518, 550, 588	426, 560, 600	285, 365, 390	345	340
fluorescence (nm)	**H_2P^{8-}**: 658	**ZnP^{8-}**: 612	**pyrene**$^+$: 500	**pyrene**$^+$: 500 **H_2P^{8-}**: 658	**pyrene**$^+$: 500 **ZnP^{8-}**: 612	no emission	658, 715	612, 665	500	373	365
fluorescence lifetime (ns)	**H_2P^{8-}**: 0.25 ± 0.05	**ZnP^{8-}**: 0.2 ± 0.05	**pyrene**$^+$: <0.1	**pyrene**$^+$: <0.1 **H_2P^{8-}**: 9.4 ± 0.5	**pyrene**$^+$: <0.1 **ZnP^{8-}**: 2.1 ± 0.2	no emission	9.4 ± 0.5	2.1 ± 0.2	2.7 ± 0.5 (water); 13.5 ± 2.0 (THF)	109 ± 5	650 ± 20
fluorescence quantum yields	**H_2P^{8-}**: 0.003	**ZnP^{8-}**: 0.005		**H_2P^{8-}**: 0.11	**ZnP^{8-}**: 0.04		0.11	0.04	0.01	0.07	0.65
differential absorption spectra (nm)	470 (max) 520 (min) 560 (min) 650 (min)	475 (max) 570 (min) 640 (max)	460 (max) 550−800 (bleaching)	not measured	not measured	450−800 (bleaching) 670 (max)	470 (max) 520 (min) 560 (min) 650 (min)	475 (max) 570 (min) 640 (max)	460 (max) 520−620 (bleaching)		
singlet lifetimes	**H_2P^{8-}**: 210 ± 5 ps	**ZnP^{8-}**: 160 ± 5 ps	**pyrene**$^+$: 1.5 ± 0.2 ps	not measured	not measured		10.2 ± 0.5 ns	2.3 ± 0.2 ns	stable up to 1.5 ns		
singlet excited-state energy (eV)	**pyrene**$^+$: 2.7 **H_2P^{8-}**: 1.9	**pyrene**$^+$: 2.7 **ZnP^{8-}**: 2.1	**pyrene**$^+$: 2.7	**pyrene**$^+$: 2.7 **H_2P^{8-}**: 1.9	**pyrene**$^+$: 2.7 **ZnP^{8-}**: 2.1		1.9	2.1	2.7	3.2	3.2
$E_{1/2}$ (V)			**SWNT**: −0.15;[a] +0.6[a] **pyrene**$^+$: +0.9[a]			−0.15[c]	+0.94[b]	+0.77[b] −1.42[b]	+1.3[a]		
triplet abs. (nm)							780	860	650	445	
radical ion pair lifetime (μs)	0.65 ± 0.05	0.4 ± 0.05									

[a] Assuming E(quasi-reference Ag electrode) = −0.1 V (vs SCE). [b] Reference 25. [c] Reference 6e.

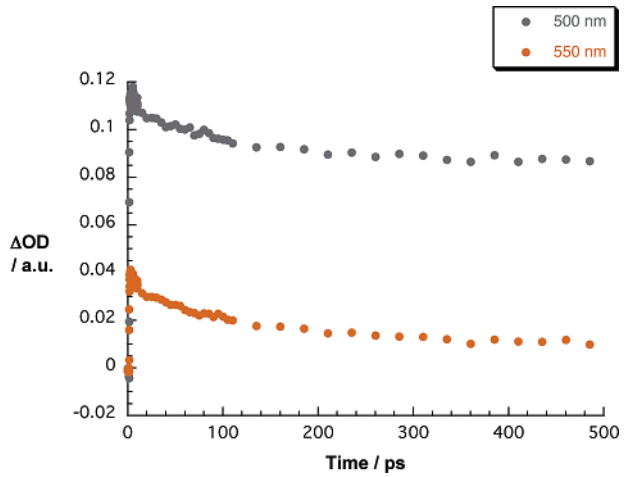

Figure 9. Time-absorption profiles at 500 and 550 nm following photoexcitation of **SWNT/pyrene^{+}/ZnP^{8-}** in nitrogen-saturated aqueous solutions, monitoring the charge separation evolving from the ZnP singlet excited state.

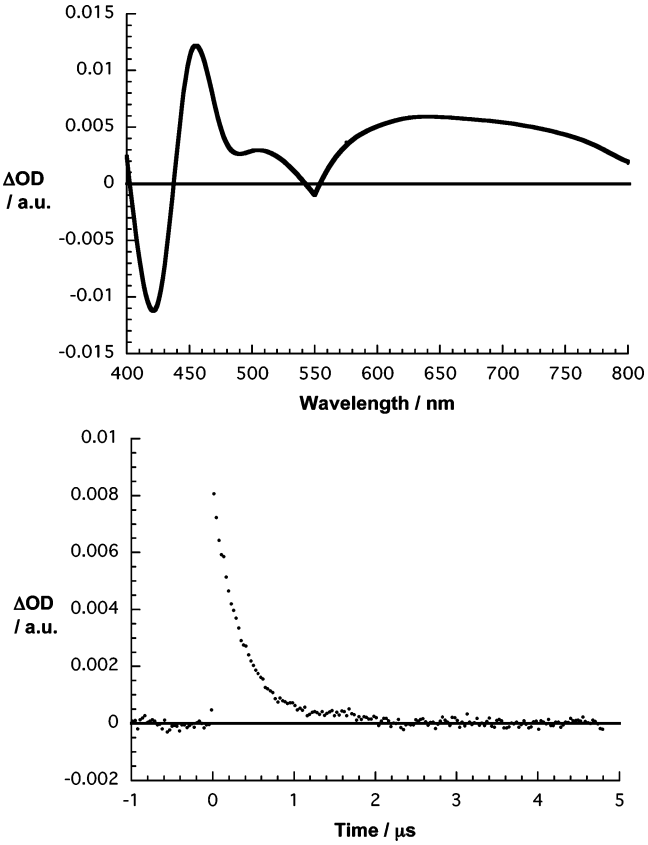

Figure 10. Differential absorption spectrum (top; vis and NIR) obtained upon nanosecond flash photolysis (532 nm) of **SWNT/pyrene^{+}/ZnP^{8-}** in nitrogen-saturated aqueous solutions with a time delay of 100 ns (taken from ref 6b) and time-absorption profiles (bottom) of the spectrum shown above at 650 nm.

component. In particular, lifetimes that are nearly on the order of microseconds (0.4 ± 0.05 μs) were derived from the decays of the oxidized donor in the 600−800 nm range. In the corresponding **SWNT/pyrene^{+}/H$_2$P^{8-}**, a slightly longer lifetime of 0.65 ± 0.05 μs was established.

A summary of all the photophysical and electrochemical data discussed in this work, together with some others only given for sake of completeness, is shown in Table 1.

Table 2. Summary of the Molecular Dynamics Results for the Interaction with Pyrene[a]

system	radius	inverse radius	energy (opt)	$\Delta H_{298\ K}$	$\Delta F_{298\ K}$	$\Delta S_{298\ K} = T(\Delta F - \Delta H)_{298\ K}$
C_{60}	3.56	0.281	−10.26	−8.67	−6.64	−0.60
(5,5)	3.42	0.293	−16.67	−14.64	−11.78	−0.85
(9,0)	3.57	0.280	−16.83	−14.95	−11.77	−0.95
(8,8)	5.44	0.184	−18.39	−16.32	−12.98	−1.00
(14,0)	5.51	0.182	−18.45	−16.41	−13.04	−1.00
(17,0)	6.68	0.150	−19.17	−17.02	−13.92	−0.92
(10,10)	6.79	0.147	−19.18	−17.10	−13.93	−0.94
(12,12)	8.14	0.123	−19.87	−17.73	−14.38	−1.00
(15,15)	10.18	0.098	−20.57	−18.42	−14.87	−1.06
(17,17)	11.53	0.087	−20.98	−18.76	−15.17	−1.07
graphene sheet	∞	0.000	−24.70	−21.85	−17.81	−1.20

[a] Radii in Å, inverse radii in Å^{-1}, energies in kcal mol^{-1}; entropy in cal mol^{-1} K^{-1}.

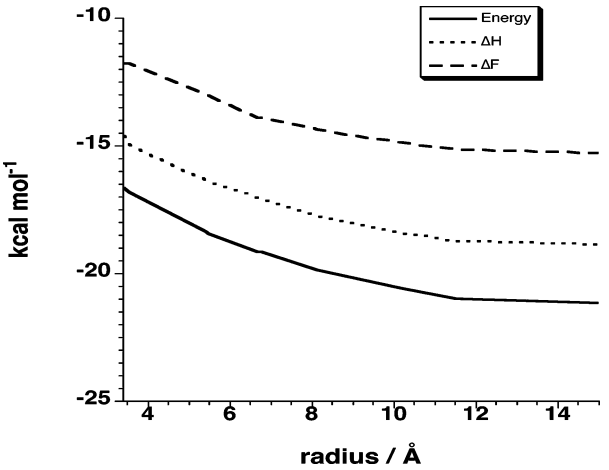

Figure 11. Calculated potential energy, enthalpy, and free energy at room temperature versus SWNT radius.

More on SWNT/Pyrene. An issue that the photophysical and electrochemical investigations presented above could not address is the size of the interactions between **SWNT** and **pyrene**. These interactions are, however, fundamental to understand the dispersion of **SWNT**s. For example, as the radius of **SWNT**s decreases, one might qualitatively expect weaker interactions with the planar and rigid structure of **pyrene**. One of the major difficulties in properly evaluating the **SWNT/pyrene** interaction is the high mobility that **pyrene** shows on the surface of **SWNT**. Upon adsorption, small movements of the organic moiety readily break the $\pi-\pi$ stacking interactions, which, however, are immediately re-formed a fraction of an angstrom away. To address this issue, free energies were calculated by integrating the potential mean force (PMF) curves,[18] which were obtained by molecular dynamics simulations (200 ps *NVT* molecular dynamics) at 298 K. Potential energies, on the other hand, were calculated with a model that we have employed previously in the investigation of interactions in and with nanotubes.[19] The distances between the center of mass of a pyrene molecule and (i) the center of mass of C_{60}, (ii) the axis of the tube, or (iii) the plane of the graphene layer were constrained to different values. Distances up to 12 Å, spaced by 0.125 Å, were sampled. The average forces at each distance were then integrated to obtain the work for adsorption or free energy.

(18) Pearlman, D. A.; *J. Chem. Phys.* **1993**, *91*, 11.

Table 2 shows a summary of the results. As expected, the free energy of adsorption of **pyrene** is minimal for C_{60} and maximal for a graphene sheet. The optimized energy, the enthalpy, and the free energy at 298 K show similar trends, Figure 11. If C_{60} and graphene are excluded, the plot of the various types of energies versus the inverse of the radius is linear. From the narrow (5,5) to the wider (17,17) SWNTs, the radius varies by more than a factor of 3, while the various types of energy of interaction change by ~1.5 times. The several kilocalories per mole of difference suggest that the majority of the properties reported here belong to **SWNT** that have the larger radius in the sample and may not be relevant to those with narrower diameters.

Conclusions

In this work, we have explored the consequences of single wall carbon nanotubes interacting with a pyrene derivative and two water-soluble porphyrins, on the basis of photophysical and electrochemical experiments. A detailed summary of ground- and excited-state interactions between the individual building blocks of Scheme 1 is presented in the case of single wall carbon nanotubes (**SWNT**), 1-(trimethylammonium acetyl) pyrene (**pyrene**$^+$), and 5,15-bis-[2′,6′-bis-{2″,2″-bis-(carboxy)-ethyl}-methyl-4′-*tert*-butyl-pheny]-10,20-bis-(4′-*tert*-butylphenyl) porphyrin octasodium salt and the related zinc complex (**H_2P^{8-}** and **ZnP^{8-}**). Three aspects are particularly important. First, **SWNT** and **pyrene**$^+$, which both aggregate heavily in aqueous media, give rise to a remarkably stable **SWNT/pyrene**$^+$ hybrid. Interestingly, experimental evidence (i.e., AFM for **SWNT** and fluorescence for **pyrene**$^+$) is found that suggests that in **SWNT/pyrene**$^+$ both constituents are monomeric. Second, rather long-lived radical ion pairs (i.e., microseconds) are formed upon electronic excitation of the porphyrin moieties in **SWNT/pyrene**$^+$**/ZnP**$^{8-}$ and **SWNT/pyrene**$^+$**/H_2P^{8-}**. Third, modeling shows that the data are likely to be relevant to the SWNTs present in the sample that possess wider diameters.

Experimental Section

Femtosecond transient absorption studies were performed with 387 nm laser pulses (1 kHz, 150 fs pulse width) from an amplified Ti: sapphire laser system (Clark-MXR, Inc.). Nanosecond laser flash photolysis experiments were performed with 337 nm laser pulses from a nitrogen laser (8 ns pulse width) in a front face excitation geometry. Fluorescence lifetimes were measured with a Laser Strope fluorescence lifetime spectrometer (Photon Technology International) with 337 nm laser pulses from a nitrogen laser fiber-coupled to a lens-based T-formal sample compartment equipped with a stroboscopic detector. Details of the Laser Strobe systems are described on the manufacture's web site. Emission spectra were recorded by using a FluoroMax-3 (Horiba Company). The experiments were performed at 20 °C.

Millipore water was used for the preparation of solutions for electrochemical investigations. Na_2SO_4 or $LiClO_4$ (pro analysi from Merck) were used as supporting electrolyte in some experiments.

Electrochemical Instrumentation and Measurements. The electrochemical experiments were carried out with an Autolab (EcoChemie) model PGSTAT30 with a platinum disk (diameter 10 μm) as working electrode, a platinum spiral as counter electrode, and a silver wire as quasi-reference electrode. Temperature control was accomplished within 0.1 °C with a Lauda RL 6 CS thermostat.

TEM Analyses. A drop of the solution of **SWNT/pyrene**$^+$ in water was placed on a copper grid (3.00 mm, 200 mesh, coated with carbon film). After air-drying, the sample was investigated by TEM Philips EM 208, accelerating voltage of 100 kV.

AFM Analyses. The samples were prepared by spin coating on silicon wafers from a solution of **SWNT/pyrene**$^+$ in water and then investigated with a Veeco multimode scanning probe microscope equipped with a Nanoscope IIIa controller. This technique allows the almost complete dispersion of the nanotubes.

To describe the carbon structure, we employed the Brenner potential.[20] The van der Waals interactions were described by the relevant part of the MM3 potential.[21] All the calculations were performed with a modified version of the TINKER molecular mechanics/dynamics software package.[22−24]

Preparation of SWNT/pyrene$^+$**.** Water-soluble **SWNT** were obtained in analogy to previous work, using 1-(trimethylammonium acetyl) pyrene (**pyrene**$^+$).[5e] In particular, 0.25 mg of **SWNT** and 1.0 mg of **pyrene**$^+$ were dissolved in 5 mL of H_2O and stirred at room-temperature overnight. Next, the suspension was kept in a temperature-controlled (20 °C) sonication bath (115 W) for 1 h. To reduce the amount of free pyrene in solution, the **SWNT/pyrene**$^+$ complex was centrifuged solid (i.e., 10 000 rpm for 30 min), and decanted upon 30 min standing. The fluorescence spectrum of this supernatant solution corresponds to the black spectrum in Figures 4 and S6. Next, the solid was resuspended in H_2O, stirred vigorously overnight, sonicated for 1 h, and centrifuged at 6000 rpm. From the supernatant solution, a fluorescence spectrum, red spectrum in Figures 4 and S6, was taken. The last steps were repeated, and the resulting fluorescence spectrum is shown as the beige spectrum in Figures 4 and S6.

We have no evidence for appreciable **pyrene**$^+$ contamination with byproducts (i.e., 1-(dimethylaminoacetyl)pyrene). HiPCO **SWNT**s were purchased from Carbon Nanotechnologies Inc. (www.cnanotech.com). Solvents and chemicals were purchased form Aldrich and were used as received. The synthesis and purity of 5,15-bis-[2′,6′-bis-{2″,2″-bis-(carboxy)-ethyl}-methyl-4′-*tert*-butyl-pheny]-10,20-bis-(4′-*tert*-butylphenyl) porphyrin octasodium (**H_2P^{8-}**) salt and the related zinc complex (**ZnP^{8-}**) has been described previously.[25]

Thermogravimetric Analysis of SWNT/Pyrene$^+$**.** A solution of **SWNT/pyrene**$^+$ was centrifugate at 2000 rpm for 4 h, the supernatant was removed, and the solid was dried under vacuum overnight. The thermogravimetric analyses were performed with a TGA Q500 TA Instruments at 10 °C/min under nitrogen.

Acknowledgment. Support from EU (i.e., projects "Cassius-Clays" and "Wonderfull"), University of Trieste, MIUR (Grants PRIN 2004, prot. 2004035502), FIRB project (i.e., "Carbonio Micro e Nanostrutturato"), DFG, SFB 583, and the Office of Basic Energy Sciences of the U.S. Department of Energy (NDRL 4677) is gratefully acknowledged.

Supporting Information Available: Fluorescence spectra, differential absorption spectrum, absorption spectra, TGA. This material is available free of charge via the Internet at http://pubs.acs.org.

JA0624974

(19) (a) Pfeiffer, R.; Kuzmany, H.; Pichler, T.; Kataura, H.; Achiba, Y.; Melle-Franco, M.; Zerbetto, F. *Phys. Rev. B* **2004**, *69*, 035404/1. (b) Melle-Franco, M.; Kuzmany, H.; Zerbetto, F. *J. Phys. Chem. B* **2003**, *107*, 6986. (c) Georgakilas, V.; Pellarini, F.; Prato, M.; Guldi, D. M.; Melle-Franco, M.; Zerbetto, F. *Proc. Natl. Acad. Sciences* **2002**, *99*, 5075. (d) Melle-Franco, M.; Prato, M.; Zerbetto, F. *J. Phys. Chem. A* **2002**, *106*, 4795. (e) Leyton, P.; Gomez-Jeria, J. S.; Sanchez-Cortes, S.; Domingo, C.; Campos-Vallette, M. *J. Phys. Chem. B* **2006**, *110*, 6470.

(20) Brenner, D. W. *Phys. Rev. B* **1990**, *42*, 9458.
(21) Allinger, N. L.; Yuh, Y. H.; Lii, J.-H. *J. Am. Chem. Soc.* **1989**, *23*, 8551.
(22) Ponder, J. W.; Richards, F. J. *J. Comput. Chem.* **1987**, *8*, 1016.
(23) Kundrot, C. J.; Ponder, W.; Richards, F. J. *J. Comput. Chem.* **1991**, *12*, 402.
(24) Dudek, M. J.; Ponder, J. W. *J. Comput. Chem.* **1995**, *16*, 791.
(25) See for details: (a) Jux, N. *Org. Lett.* **2000**, *2*, 2129. (b) Guldi, D. M.; Zilbermann, I.; Anderson, G.; Li, A.; Balbinot, D.; Jux, N.; Hatzimarinaki, M.; Hirsch, A.; Prato, M.; *Chem. Commun.* **2004**, 726.